Nuclear Physics Experiments: α-spectroscopy*

Craig Reingold†
Department of Physics,
The University of Notre Dame

Patricia Huestis‡ and Shane Moylan§
Department of Physics,
The University of Notre Dame

(Experimental Methods in Physics, Spring 2016)
(Dated: February 1, 2016)

Detection of charged particles is a vital skill for the modern research scientist. In this paper, we will discuss the process of α-particle spectroscopy. We will go through calibration techniques, and using α-particle energies to identify the parent radiation source. Finally, we will use measured ΔE_α to determine the thicknesses of various foils.

While we were successfully able to calibrate our detector and identify and unknown radiation source, the methods outlined in this paper are insufficient for professional quality research. We also found the calculation of foil thickness to be unreliable for large $\Delta E/E$ ratios.

I. INTRODUCTION

Since the discovery of the nucleus, radiation detection has been a fundamental facet of experimental nuclear physics. In fact, it was detecting α-particles that lead to the discovery of the nucleus as we know it. Radiation detection grants us the ability to study everything from the very structure of nucleons to the inner workings of the stars. Therefore, it is essential for the modern research physicist to thoroughly understand radiation detection.

In this paper, we will focus on detection of massive, charged particles using solid-state semiconductor detectors. Specifically, we will be detecting and determining the energy of α-particles emitted from radioactive decay of various nuclei. This process is commonly referred to as α-spectroscopy.

A. Nuclear Decay

During α-decay, the original (parent) nucleus emits an ionized ^{4}He nucleus, as seen in Equation 1. This type of decay is caused by electrostatic repulsion, and quantum tunneling [2].

$$ {}^{A}_{Z}N \rightarrow {}^{A-4}_{Z-2}M^* + {}^{4}_{2}\mathrm{He} \qquad \left({}^{4}_{2}\mathrm{He} = \alpha\right) \tag{1} $$

Within a typical nucleus, there are two primary contributing factors to the nuclear potential. There is the attractive potential generated by the strong interaction between nucleons, and a repulsive potential generated by the electrostatic interaction between nucleons (*See Figure 1*). Classically, if a particle is found on either side

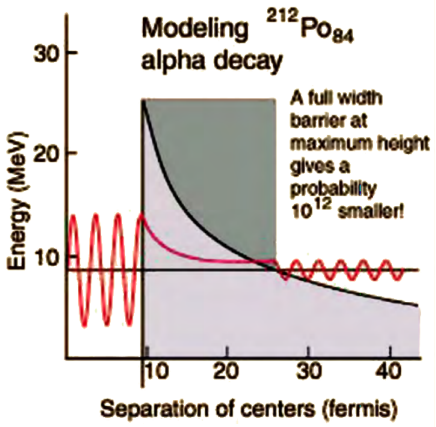

FIG. 1. An example of quantum tunneling. [1] The particle begins on the left side of the barrier, bound to the nucleus. It then tunnels through the barrier, losing energy, and exits the barrier on the other side, with less energy.

of the potential, and has insufficient energy to overcome the potential barrier, as seen by the solid horizontal line in Figure 1, the particle will stay on that side. Since we are working at the subatomic scale, however, these nucleons will behave quantum mechanically.

As long as the barrier in not infinite, there is a non-zero probability of the particle subject to this potential being found within the barrier. The particle will, however, lose energy in the barrier. This means that

* from *Advanced Physics Laboratory Manual*, [1]
† Primary Author,NSH 284, creingol@nd.edu
‡ NDRL 316, phuestis@nd.edu
§ NSH 284, smoylan1@nd.edu

there will be particles with enough energy to completely tunnel through the barrier, and exist outside the nucleus.

Clusters of α-particles are known to exist in nuclei, given the stability and high binding energy of the ^{4}He nucleus. This stability arises from the fact that the proton and neutron numbers of this nucleus are shell closures in the nuclear shell model.

If a nucleus has a high-energy α-cluster in or near a valence shell, there is a non-zero probability it will be able to tunnel through the nuclear potential. It will then be accelerated away from the nucleus by electrostatic repulsion between the emitted α-particle and the remaining protons in the nucleus.

If a nucleus has a high-energy α-cluster in or near a valence shell, there is a non-zero probability it will be able to tunnel through the nuclear potential. It will then be accelerated away from the nucleus by electrostatic repulsion between the emitted α-particle and the remaining protons in the nucleus.

II. APPARATUS & PROCEDURE

A. Apparatus

For this experiment, we elected to use a solid-state silicon detector. Experiments were conducted with a ^{241}Am mixed source. The radioactive material mixed with the ^{241}Am was to be determined in a later part of the experiment (See Section III B).

A block diagram[1] of our apparatus can be found in Figure 2. We were able to achieve appropriate vacuum in our target chamber using only a roughing pump. An evacuated target chamber was essential to our experiment, due to the high probability of the α-particles radiated from the decaying nuclei interacting electromagnetically with the electrons in the atmosphere. If the α-particles were to interact with the electrons, it would result in either a loss of kinetic energy, or a loss of ionization. An unionized α-particle will not be able to interact with the Si lattices in the solid-state detector, and will therefore be unable to generate a current in the detector.

For the final part of our experiment (See Section II.B, Subsection 3), we also used thin foils. We used thin aluminum foils (4 μm and 7 μm), and thin havar foils (2.3 μm and 4.6 μm). All analysis was performed using ROOT [3] and SRIM [4]. SRIM allowed us to calculate $\frac{dE}{dx}$ for aluminum and havar without needing to explicitly solve the Bethe formula for charged particle interaction with matter.

[1] Block diagram generated by P. Huestis

B. Procedure

This experiment was conducted in three parts [1]. Before taking any usable data, we first needed to calibrate our detector. After calibration, we were able to identify an unknown radioactive isotope by identifying the kinetic energy of the α-particle emitted from the isotope. Finally, we used our calibrated detector and known α-sources to determine the thickness of various foils using the Bethe formula.

1. Calibration

After amplification, the electrical signal generated from charged particle interaction with our semiconductor detector is sent to a multi-channel analyzer. This bins all of the signals received into discrete channels, and sends them to the data acquisition system. In order to measure the energy of the α-particles, we need to find a mathematical relation between channel number and the energy the α-particle deposited in the detector.

Before we are able to determine this calibration, we must first determine the optimal bias voltage to apply across our detector. We were able to accomplish this by minimizing our measured resolution as a function of bias voltage.

$$R = \frac{FWHM}{\mu} \qquad FWHM = 2\sqrt{2\ln 2}\sigma \tag{2}$$

Resolution (R) was calculated by fitting Gaussian functions to our unknown, single peak, and then using Equation 2 with the given fit parameters (μ and σ).

Once our detector was operating at the correct voltage, we were able to fit a double Gaussian to the channels where the ^{241}Am α-particles deposited their energy. Since the energies of these particles are well known, we were able to perform a rough linear calibration using the μ and σ values from the fitting procedure.

2. Spectroscopy

After finding a rough, two-point calibration, we were able to determine a range of possible E_α values for the unknown detected particle. We were then able to search for a well known α-source emitting in this energy range,

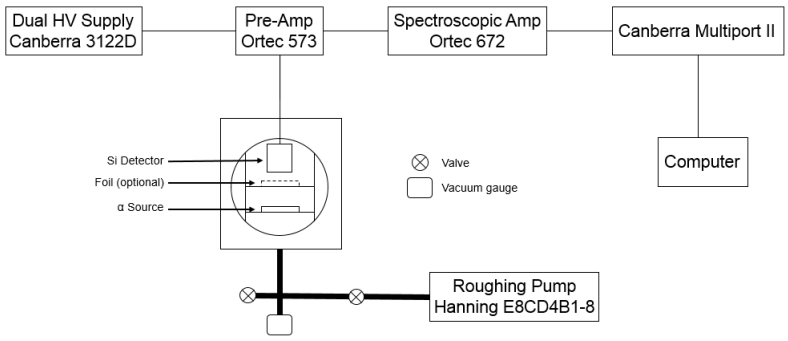

FIG. 2. A block diagram of our apparatus. From left to right, our experiment required the use of a high voltage supply, a pre-amplifier for the solid-state detector, a spectroscopic amplifier, a multi-channel analyzer, and finally a data acquisition software running in a computer. Inside of our target chamber, we have our solid-state silicon detector, a shelf for holding thin foils above the source, and then a shelf to house the source.

with a reasonable half life. [5] Thus, we were able to identify an unknown radioactive isotope by measuring the energy of the α-particle emitted.

After determining the unknown source, we were able to fit a single Gaussian function to this peak. Using these fit parameters, and the fit parameters from the initial calibration, we were able to generate a three-point linear calibration.

3. Energy Loss in Material

The final objective of this experiment was to determine thickness of a foil using α-particles. The rate of energy loss of a charged particle as a function of distance though a material has been well studied. The differential equation, the Bethe Equation, describing this rate can be found in Equation 3.

$$-\frac{dE}{dx} = \frac{4\pi}{m_e c^2}\frac{nz^2}{\beta^2}\left(\frac{e^2}{4\pi\epsilon_0}\right)^2 \times \left[ln\left(\frac{2m_e c^2\beta^2}{I\cdot(1-\beta^2)}\right) - \beta^2\right] \quad (3)$$

This equation is only solveable analytically, since E is a function of β. We therefore need a way of solving the Betha equation analytically in order to proceed.

By using SRIM to analytically solve for $\frac{dE}{dx}$ for α-particles passing through a foil with a known elemental composition, and approximating $\frac{dE}{dx}$ to be constant, we were able to estimate the foil thickness by Equation 4.

$$\Delta x = \frac{dE}{dx}\cdot\Delta E \quad (4)$$

We were able to determine ΔE by measuring the final energy of an emitted α-particle after passing through a thin foil, and subtracting this from the known initial energy of the particle. It is also worth noting, and will be discussed in later sections, that this is only an appropriate method for determining foil thickness if ΔE is not a significant fraction of the total E_α. If ΔE is appreciable, we can no longer approximate $\frac{dE}{dx}$ as constant, and Equation 4 is longer valid.

III. DATA & ANALYSIS

A. Calibration

Figure 3 shows our measured resolution as a function of bias voltage. Resolution was calculated using Equation 2, and associated uncertainty [6] with Equation 5.

$$\delta R = R\cdot\sqrt{\left(\frac{\delta\mu}{\mu}\right)^2 + \left(\frac{\delta\sigma}{\sigma}\right)^2} \quad (5)$$

It is clear from this figure, and the fit function, that the minimum resolution is achieved at an infinite bias. However, this is not only impractical, but would supersaturate the band-gap of the silicon Therefore, a bias voltage of 75 V was selected for the remainder of data taken.

In order to determine the calibration parameters, it is necessary to fit a first order polynomial to a plot of known E_α's and the channel these α-particles were binned into after detection. We were able to determine the channel the α-particles were detected in by fitting a double

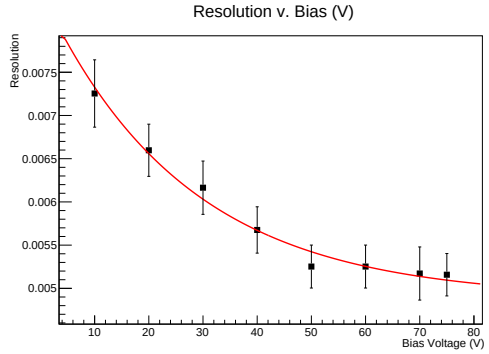

FIG. 3. Detector resolution as a function of bias voltage across the detector. The function fit over the data, for illustrative purposes only, is $f(x) = C_0 - C_1 e^{-C_2 x}$, for $C_0, C_1, C_2 \in \mathbb{R}^{(+)}$

Gaussian to the two ^{241}Am peaks. An example of this can be found in Figure 4. Our fitting algorithm uses χ^2 minimization to determine an optimal fit for the data [3].

A double Gaussian function was deemed appropriate due to the close proximity of the two peaks. Fitting both peaks simultaneously with six free parameters (amplitude, mean, and standard deviation for each peak) decreases the uncertainty in the fit relative to fitting each peak individually. Since there is clear overlap between the high energy tail of the smaller peak, and the low energy tail of the larger peak, trying to fit the two peaks individually will lead to a systematic error. Fitting a linear combination of two Gaussian distributions in parallel removes this error.

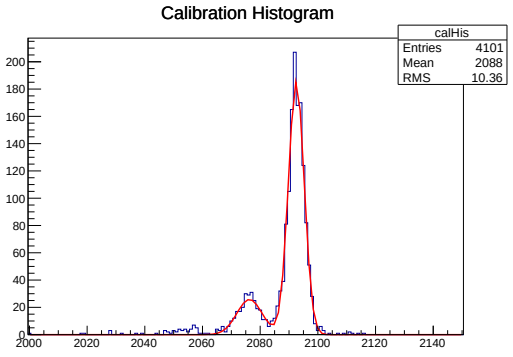

FIG. 4. Example of the double Gaussian function being fit to the two primary α-particle energies from ^{241}Am. The double Gaussian is simply a convolution of two Gaussian distributions, however, fitting both simultaneously with a double Gaussian minimizes the uncertainty associated with overlap between the two peaks.

B. Spectroscopy

We can now, using our rough calibration from the previous section, generate a range of E_α's to search over. Since α-decay is a quantum mechanical process, there is ideally one energy that all α-particles from a specific decay are emitted at. Therefore, the E_α measured should act like a fingerprint, leading us back to the parent nucleus.

We looked over a range of E_α centered around 3.14 MeV, over a window of about 250 keV. [5] After ruling out parent nuclei with inappropriately short half-lives, and with count rates so low they would essentially be undetectable, we were able to determine our unknown α-source. The α-source used in this experiment was a mixture of ^{241}Am and ^{148}Gd.

Parent	E_α (MeV)	I_α (%)
^{148}Gd	3.182	100.0
^{241}Am	5.443	13.0
	5.486	84.5

TABLE I. Elemental composition of the radioactive source. The table includes the parent nucleus, the energy of the radiated α-particle, and the relative intensity for each α-particle

Once the composition of the target is well known, we can easily determine the exact values of the three energy peaks in our measured spectrum. Therefore, we can do a three point linear calibration for higher precision. The calibration is done by fitting a single Gaussian to the ^{148}Gd, and using the μ and σ from all three visible peaks, performing a χ^2-minimization fit of a first order polynomial on the data. This gave us the linear calibration:

$$E_\alpha = 42.3 \text{ keV} + 2.60 \frac{\text{keV}}{\text{ch.}} \cdot [ch.]$$

The above calibration calibration was then applied to every subsequent spectrum. A full, calibrated spectrum can be found in Figure 6.

C. Energy Loss in Material

After proper calibration of the detector, we can proceed to the final phase of this experiment, where we attempt to determine the thicknesses of various foils. Figure 5 shows three histograms superimposed on each other, so we can track the shape of the E_α peak as it travels through aluminum. The figure clearly illustrates not only the energy loss as we increase the thickness of the foil, but also the decrease in the number of particles detected. This decrease is seen by the steadily decreasing

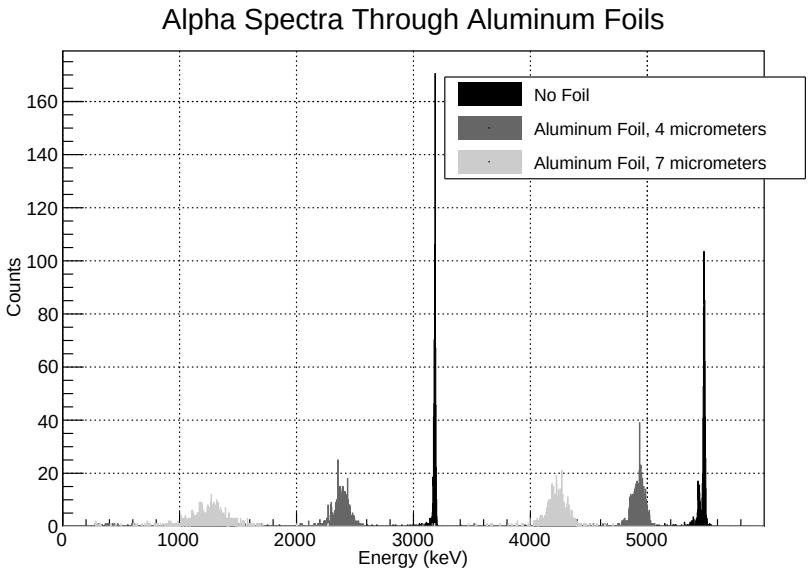

FIG. 5. Tracking the energy loss of α-particles through various thicknesses of aluminum. The three spectra all show E_α histograms, and all have identical detector live times. The graph illustrates not only an energy shift due to loss in the material, but a decrease in transmission through the material as well.

amplitude of the peaks as the foil thickness increases. We can also see the standard deviation of the peaks increase as the thickness of the foil increases. Finally, there is a noticeable difference in the energy lost by the 3.18 MeV α-particles, and the 5.4 MeV α-particles. It is clear the higher energy α-particles have a higher probability of transmission through the foil, and lose a smaller fraction of their energy in the foil.

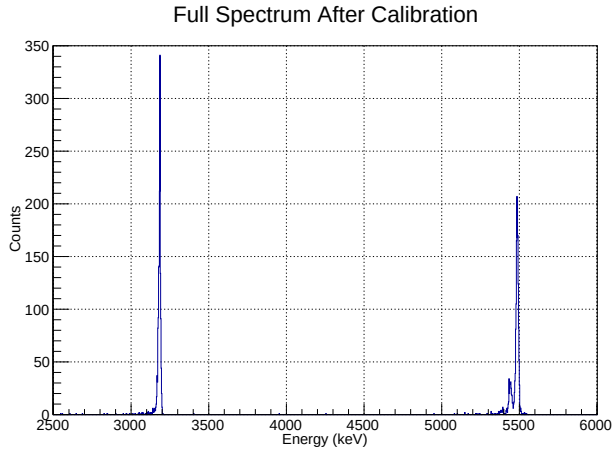

FIG. 6. Full spectrum after calibration. This allows us to verify the validity of our linear calibration graphically, by confirming that each E_α peaks appears where it should on the spectrum. Relative resolution should be unaffected, since the histogram above has the same number of bins as the uncalibrates spectrum.

To determine foil thickness, each of the peaks from the spectra taken with a foil between the source and the detector was fit with a Gaussian distribution, to determine the mean E_α after interacting with the foil. This E_α can be found in Table II. These energies were then subtracted from the initial radiated α-particle energies. In the case of the ^{241}Am doublet, the energies were compared to the average of the two original peaks, weighted by each peak's relative intensity (Table I). The calculated thicknesses can be found in Table II. Appropriate $\frac{dE}{dx}$ values were calculated using SRIM [4].

IV. DISCUSSION & CONCLUSION

Measuring the energy of charged particles is a fundamental component of modern experimental nuclear physics. Through this experiment, we were successfully able to measure the energies of α-particles incident on a solid-state detector. We were also able to find methods within our analysis to improve on this technique for future research endeavors.

After our calibration, we were immediately able to recognize areas of improvement. Beginning with the resolution data acquisition, it became apparent that long runs were necessary for low-statistics peaks. While Figure 4 shows a good fit of the double Gaussian, original runs did not look this great. We almost doubled our detector live time for the calibration run depicted in Figures 4 and 6 from the times we originally thought

Film	E_0 (keV)	E_f (keV)	Thickness (calc) (μm)	Quoted (μm)
Aluminum	3182	2385.35	3.77 ± 0.287	4.0
	3182	1257.90	9.10 ± 0.847	7.0
	5480	4929.35	3.57 ± 0.306	4.0
	5480	4232.10	8.10 ± 0.495	7.0
Havar	3182	1885.46	2.65 ± 0.106	2.3
	3182	459.75	5.57 ± 0.188	4.6
	5480	4581.27	2.51 ± 0.116	2.3
	5480	3685.50	5.01 ± 0.188	4.6

TABLE II. Calculated foil thicknesses from energy loss measurements. The calculated thickness tends to be closer to the quoted thickness when ΔE is not a significant fraction of the original energy. Our calculations are dependent on our assumption that $\frac{dE}{dx}$ is constant. This is only a good assumption for relatively small values of ΔE. This is reflected in the data, since the calculated thicknesses are not as good when the shifted energy is significantly lower than the original energy.

appropriate when we began taking data.

Since we are dealing with a radiation source with a half-life significantly larger than our detector's live time, it is reasonable to approximate the source's decay rate as constant. Therefore, running our detector for twice as long should double our statistics. With higher statistics, we are easily able to fit our histograms with minimal uncertainty.

Fitting procedures are always more precise with higher statistics. It is for this reason that, in the future, we will use more than two or three peaks for our energy calibration of a detector. While a three point linear calibration is acceptable for this experiment, detectors used for publishable research use substantially more known peaks to perform an energy calibration. Aside from achieving better precision with higher statistics, more known E_α's to calibrate to would have shown us whether a linear calibration was appropriate for our detector. It is nearly impossible to determine if a second order polynomial, or a linear combination of a polynomial and an exponential, would be a more appropriate fit function with barely three data points.

Finally, we look at the α-particle interaction with thin foils. As stated before, the only time it is justifiable to approximate $\frac{dE}{dx}$ to be constant is when the energy lost in the material is not appreciable. This point is illustrated clearly in Table II. When the shifted energy is closer to the original energy, and the ratio of ΔE to E_0 is small, our calculated thicknesses are closer to our quoted thicknesses. While there is still a possibility of systematic error arising from knowing the precision of the quoted thickness, there is still a more appropriate method for measuring foil thicknesses with α-particles.

During our foil thickness calculations, we elected to ignore the contribution to $\frac{dE}{dx}$ from α-particle interaction with the nuclei. This decision was made because this contribution is three orders of magnitude lower than the rate of energy loss with respect to distance traveled due to interaction with electrons. Including the electromagnetic repulsion from the nuclei in our foil would not be as advantageous to our foil thickness calculation as implementing a better approximation of $\frac{dE}{dx}$ for larger energy losses to the material.

This experiment offered substantial insight into charged particle spectroscopy. Since this is an essential technique for research physicists, practice with this detector and these analysis techniques is important. However, the techniques used throughout this experiment have room for improvement, and should not be directly applied to research.

[1] J. Hammer, *Advanced Physics Laboratory Manual* (Department of Physics, University of Notre Dame, 2008).

[2] K. S. Krane and D. Halliday, *Introductory Nuclear Physics* (Wiley, New York, 1988).

[3] R. Brun and F. Rademakers, Nucl. Inst. & Meth. in Phys. Res. A **389**.

[4] J. Zeigler, J. Biersack, and M. Ziegler, *SRIM, the Stopping and Range of Ions in Matter* (2008).

[5] S. Chu, L. Ekstrom, and R. Firestone, *The Lund/LBNL Nuclear Data Search* (http://nucleardata.nuclear.lu.se/toi/index.asp).

[6] J. R. Taylor, *An Introduction to Error Analysis: The Study of Uncertainties in Physical Measurements* (U Science, Sausalito, CA, 1997).